Supporting Information

Heterogenization of Phosphotungstate Clusters into Magnetic-Microspheres: Catalyst for Selective Oxidation of Alcohol in Water

Rakesh Chilivery, [†,‡] *Vahinipathi Chaitanya,* [†,‡] *Jayadev Nayak,* [†,‡] *Sameer Seth,* [†,‡]

*Rohit K Rana** [†,‡]

Email address of the Corresponding Author (Rohit K. Rana): rkrana@iict.res.in

[†] Nanomaterials Laboratory, Department of Catalysis & Fine Chemicals, CSIR-Indian Institute of Chemical Technology, Hyderabad-500007, India

[‡] Academy of Scientific and Innovative Research (AcSIR), Ghaziabad-201002, India

Number of pages: 27

Number of Figures: 15

Number of Tables: 7

Experimental Procedure

Materials:

Poly(allylamine hydrochloride) (PAH, 15 kDa; 1Da = 1g mol-1), citric acid, trisodium citrate, ferric chloride and ferrous chloride, sodium hydroxide, phosphotungstic acid ($H_3PW_{12}O_{40}.xH_2O$)(PTA), Alcohols, hydrogen peroxide (30% H_2O_2) were procured from Sigma–Aldrich and used as received. In all cases, Millipore water (18.2 MΩ) was used to prepare the solutions

Preparation of citrate capped iron oxide nanoparticles (cit@Fe_3O_4):

Citrate capped ferrite nanoparticles were synthesized using the method based on co-precipitation of Fe^{2+} and Fe^{3+} from respective salts. Typically, under nitrogen atmosphere, 100 mL sodium hydroxide (10 M) was added in to a mixture of iron chloride salts with Fe^{2+}/Fe^{3+} molar ratio of 1:2 forming an immediate dark brown/black suspension. The solution was stirred for 1 h at room temperature and heated at 90^{o}C for 1h, which resulted in the formation of a brown colloidal solution of ferrite. Then, 100 mL of trisodium citrate (0.3 M) was added and stirred for another 30 min. Subsequently, thus obtained citrate-capped iron oxide dispersion was cooled down to room temperature under continuous stirring, followed by the addition of an excess amount of acetone to precipitate the magnetic particles. The magnetic particles were washed 3-4 times with deionised water and collected with the help of an external magnet. Finally, the magnetically collected nanoparticles were washed with ethyl acetate and dried at room temperature and stored for further studies. The hydrodynamic sizes of these are in the range of 45 nm as determined from DLS.

Preparation of PTA-assembled magnetic microcapsules (PTA@MMS):

In a typical synthesis, an aqueous solution of PAH (2 mL, 2 mg mL^{-1}) was vortex mixed for 10s with citrate-functionalized Fe_3O_4 (2 mg mL^{-1}) dispersed in an aqueous solution of citrate

[28.52 mM, 2.5 mL] while keeping the charge ratio (*R* = total negative charge on citrate to the total positive charge on the PAH) maintained at 5. Thus formed PAH-citrate aggregates resulted in a cloudy brown suspension, which was further allowed to age for 15 min and then mixed with an aqueous solution of PTA (11.4 mM, 2.5 mL). After ageing for another 15 min the resultant precipitate (PTA@MMS) was then collected through an external magnet and further washed for 3-4 times with Millipore water to remove the unreacted reagents. Thus synthesized PTA@MMS were dried at room temperature and then used further for characterization and catalytic applications.

Catalytic oxidation of alcohols:

In a typical reaction, oxidation of alcohols was carried out in a 50 mL two necked round bottom flask by addition of benzyl alcohol (1 mmol), oxidants (30wt % H_2O_2 (1.5 mmol) and 20 mg of catalyst (comprises 5μmol PTA) in water solvent (6 mL) under stirring at the required temperature (90^{o}C). The products were extracted with toluene at different intervals and analysed by using gas chromatography (GC) equipped with ZB-5 column and FID detector. The catalyst was isolated from the reaction mixture with help of an external magnet and washed several times with ethanol and water. The separated catalyst was further used in the reaction under similar conditions in order to assess its reusability.

Characterization

Optical microscopic study of the samples was done with a Leica DM4000 M LED. Field emission scanning electron microscopic (FESEM) analysis was carried out using high resolution Schottky Field Emission Scanning Electron Microscope (JEOL-7610F) furnished with an energy dispersive X-ray spectrometer (AZTEC EDS, Oxford Instruments). High resolution transmission electron microscopy (HRTEM), high-angle annular dark field scanning transmission electron microscopy (HAADF-STEM) and EDS were done with a FEI

Talos F 200x microscopes (FEI, Hillsboro, Oregon USA) operated at 200 kV equipped with HAADF and Super-X EDS detectors. The samples for TEM were prepared by dispersing the material in ethanol by ultra sonication and then drop-drying onto a formvar-coated copper grid. Dynamic light scattering (DLS) technique (Malvern Zetasizer, Nano ZS) was used for the measurement of average hydrodynamic size and zeta potential of the materials. FT-IR spectra were recorded at 4000–400 cm^{-1} on a Bruker Alpha spectrometer. Confocal micro Raman spectra were recorded using a Horiba Jobin-Yvon Lab Ram HR spectrometer equipped with a 30 mW He-Ne laser source at 633 nm wavelength with a 10% filter. X-ray diffraction patterns of the synthesized MMSs were collected on a PANalytical Empyrean equipped with Pixel 3D detector. ^{31}P NMR recorded on AVANCE III-500WB, Bruker instrument operating at 202 MHz, with a 3.2 mm triple resonance (HXY) solid state probe. The measurement was carried at room temperature using 85% H_3PO_4 as standard reference. UV-Diffused reflectance spectra were recorded on a UV-vis spectrophotometer (Carry-5000). Magnetic properties of the samples were evaluated using ADE-EV9 vibrating sample magnetometer (VSM). N_2 physisorption measurements were done with Quanta chrome Nova-4000e system, for which the samples were degassed at 90^oC for 2 h prior to the measurements. Thermogravimetric analysis (TGA) was performed with a TA Q50 thermo-gravimetric analyzer in the temperature range of 35 - 800^oC with a heating rate 10^oC/min under nitrogen atmosphere. For the catalytic test, the reaction progress was monitored by gas chromatography (GC-2010, SHIMADZU) using ZB-5 column and FID detector. Elemental analysis was carried out by Inductively Couple Plasma-Optical Emission Spectroscopy (ICP-OES), Thermo Elemental, IRIS Intrepid II XDL.

Table S1. ζ potential and hydrodynamic diameter obtained from DLS measurements for cit@Fe_3O_4 nanoparticles, PAH-cit-Fe_3O_4 aggregates, and PTA@MMS at various steps of the assembly process

Measurement	citrate@Fe_3O_4 nanoparticles	PAH-cit- Fe_3O_4 aggregates	PTA@MMS
ζ Potential (mV)	-34.8	+23	-38
Average Size (nm)	10.30	92.58	300

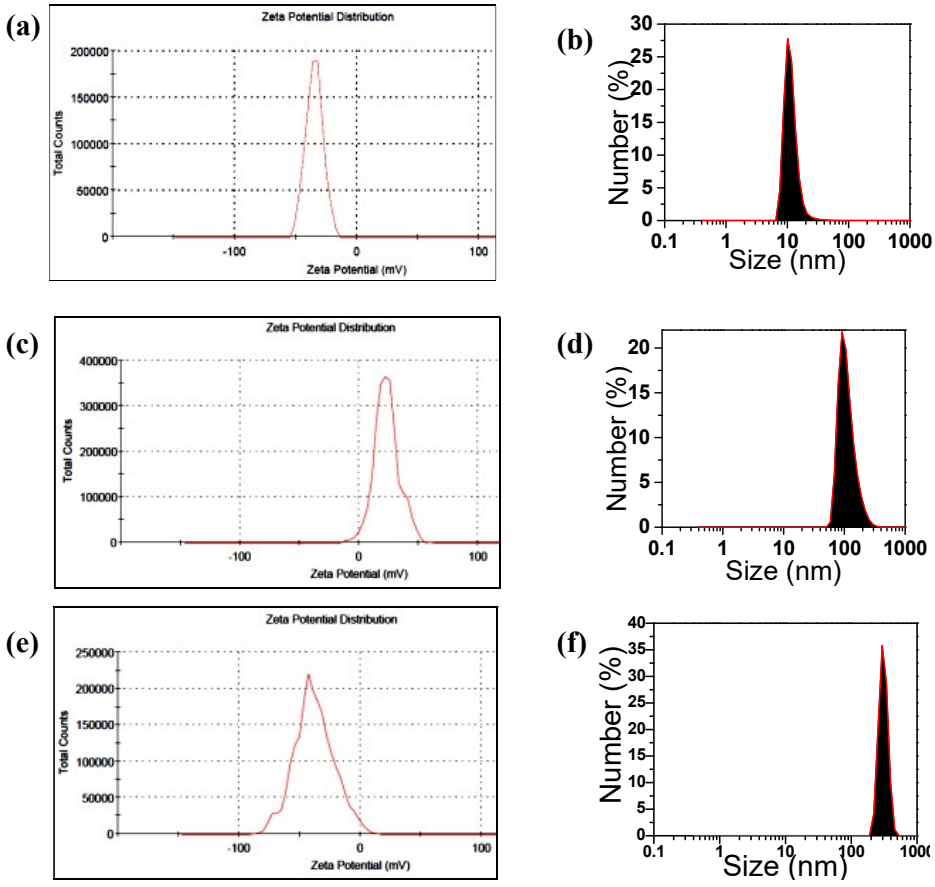

Figure S1. DLS analyses results obtained uring the assembly process: Zeta potential (a, c, e) and hydrodynamic size-distribution plots (b, d, f) for cit@Fe_3O_4 nanoparticles, PAH-cit-Fe_3O_4 aggregates and PTA@MMS samples, respectively.

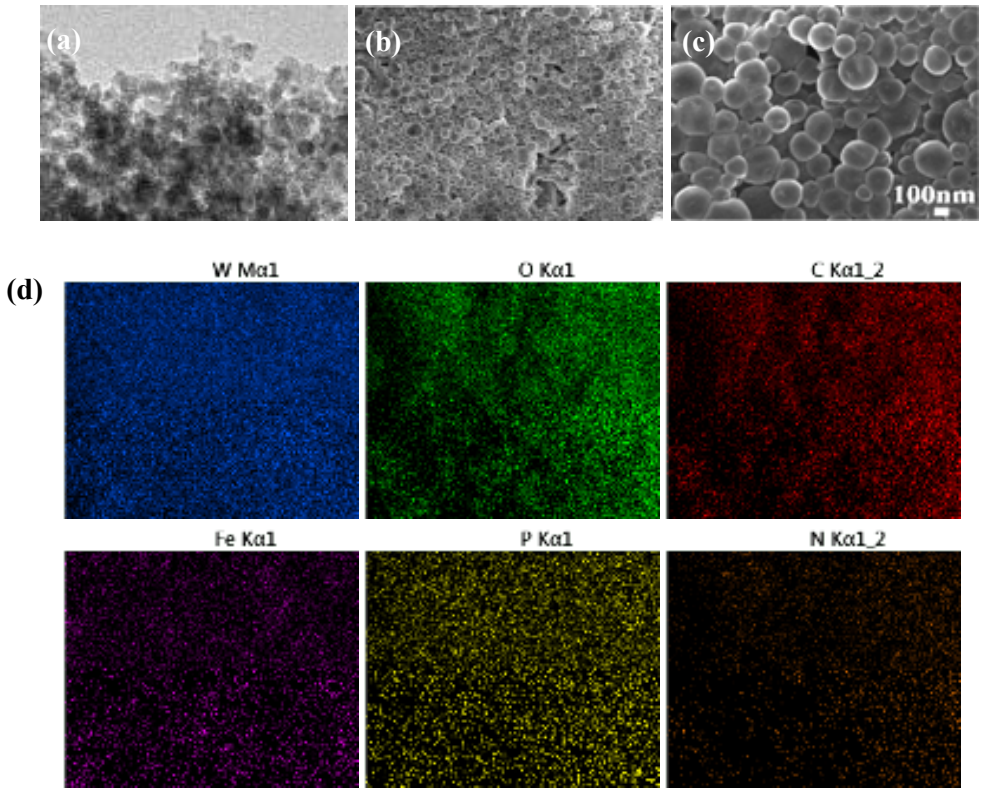

Figure S2. a) TEM image of cit@Fe_3O_4 nanoparticles; (b, c) Low and higher magnification FESEM images of PTA@MMS; d) EDS elemental mapping for PTA@MMS sample.

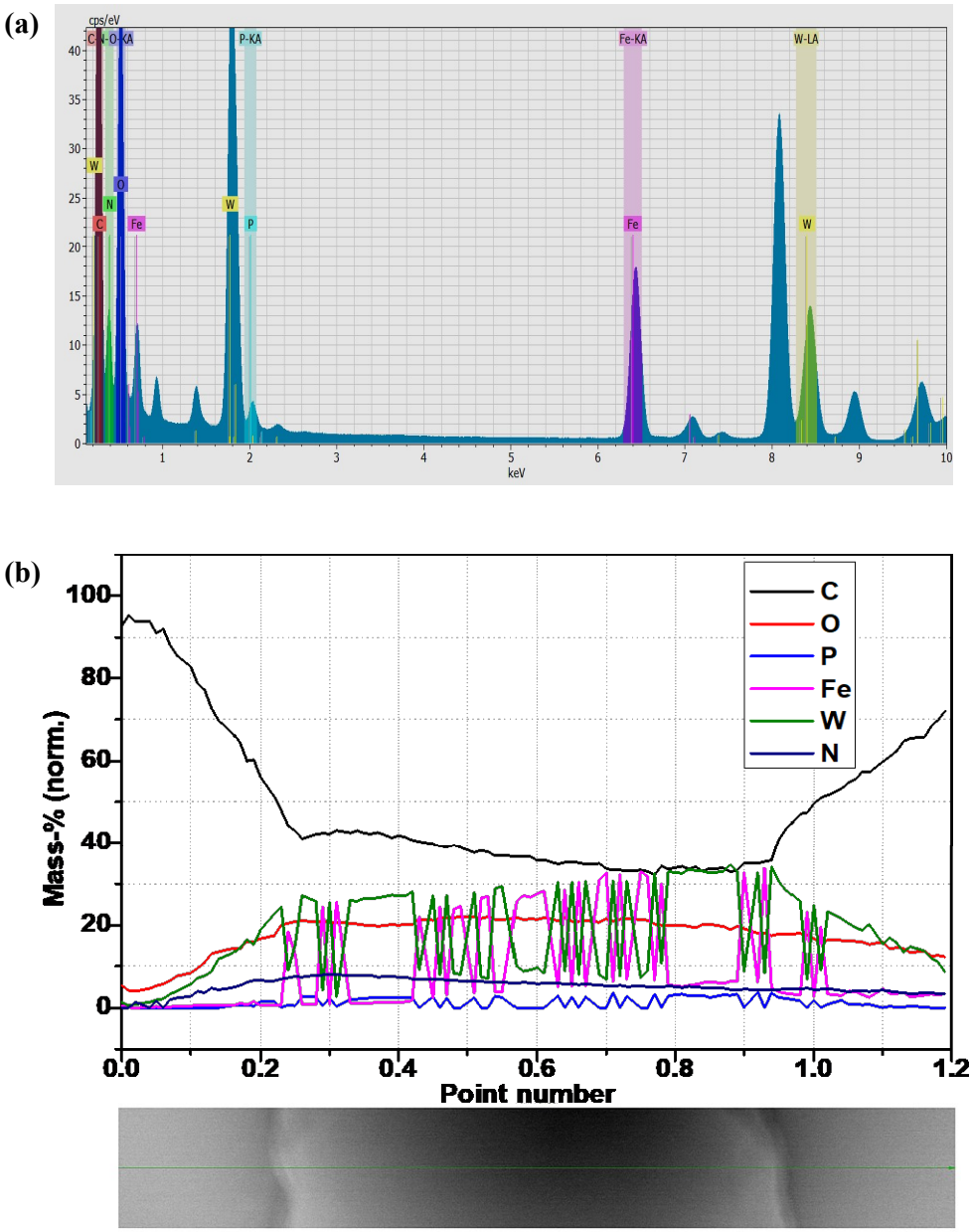

Figure S3. HAADF-STEM EDS analysis of PTA@MMS. a) EDS spectrum; b) EDS line-scan (top part) for various elements present in a sphere of PTA@MMS as shown in the HAADF-STEM image (bottom part).

Table S2. Confocal micro-Raman modes of PTA, PAH, cit@Fe_3O_4, PTA@MMS and recycled PTA@MMS samples

Sample	**Wavenumber (cm^{-1})**	**Assignment**
PTA	1008 (984), 905, 524, 216	W-O_d (terminal), W–O_b–W, W–O_c–W (bridging), W-O-W bending mode of vibration
PAH	2924	C-H stretching vibrations
cit@Fe_3O_4	672, 488, 360	Characteristic Raman modes for Fe_3O_4 [S1]
PTA@MMS (Fresh and recycled catalyst)	975 (937), 858, 511, 208 2924 599	W-O_d (terminal), W–O_b–W, W–O_c–W (bridging), W-O-W bending mode of vibration C-H stretching vibrations in PAH Fe-O stretching

* O_b represents the bridged oxygen of two octahedra sharing a corner; O_c is the bridged oxygen sharing an edge; and O_d is the terminal oxygen.

Table S3. FT-IR vibrational peak assignments for PTA, PAH, cit@Fe_3O_4, PTA@MMS and recycled PTA@MMS samples

Sample	**Wave number (cm^{-1})**	**Assignment**
PTA	1078, 984, 895, and 798	P–O_a, W–O_d, W–O_b–W, W–O_c–W
PTA@MMS (Fresh and recycled catalyst)	1076, 951, 881, and 790	P–O_a, W–O_d, W–O_b–W, W–O_c–W
	3428, 3095	-N–H stretching vibrations
	1626, 1510	-NH_2 , -NH_3^+ bending modes in PAH
	2924	C-H stretching vibrations in PAH
	1720	C=O stretching vibration in citrate
	596	Fe-O stretching in Fe_3O_4
PAH	2924	C-H stretching vibrations
cit@Fe_3O_4	596	Fe-O stretching
	1720	C=O stretching vibration

* O_a is the oxygen of the central tetrahedron; O_b is the bridged oxygen of two octahedra sharing a corner; O_c is the bridged oxygen sharing an edge; and O_d is the terminal oxygen.

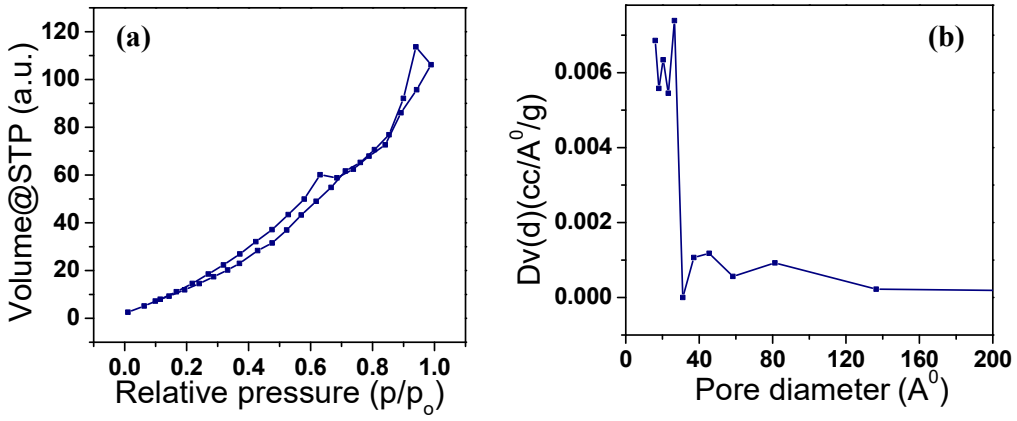

Figure S4. (a) N_2 adsorption-desorption isotherm, and (b) Pore-size distribution curve obtained from the N_2-sorption analysis of PTA@MMS**.**

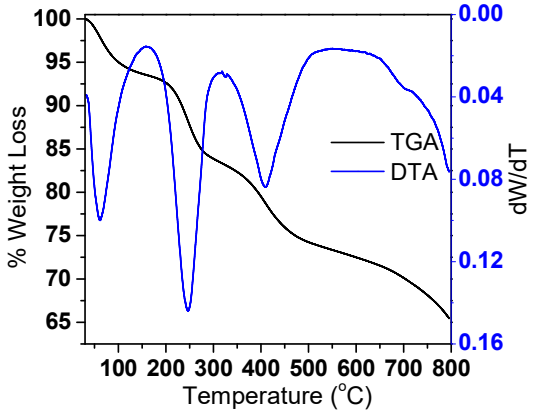

Figure S5.TG-DTA thermogram of PTA@MMS**.** The weight-loss of 8.0 Wt. % below 150 ^{o}C and 20 Wt.% within 250 – 550 ^{o}C are due to the loss of water molecules (adsorbed and crystalline), and the decomposition of organic contents, respectively. The ~3 Wt.% weight-loss in 600-700^{o}C is due to the decomposition PTA to P_2O_5, which corresponds to ~57 Wt.% WO_3 (equivalent to ~64 Wt% PTA) in PTA@MMS and the remaining ~12 Wt.% is for Fe_3O_4. Note: The weight-loss above 700^{o}C indicates the gradual but incomplete reduction of Fe_3O_4.[S2]

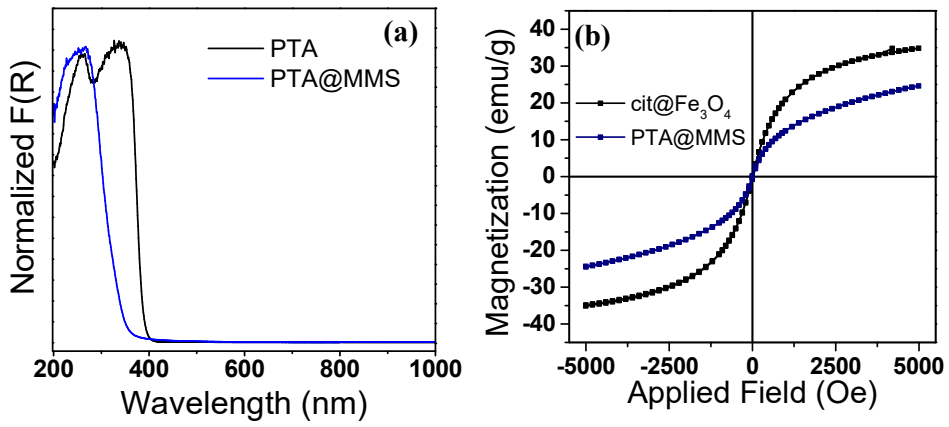

Figure S6. a) UV-Vis Diffuse reflectance spectra of PTA and PTA@MMS, and b) Vibrating sample magnetometer analysis of cit@Fe_3O_4 and PTA@MMS**.**

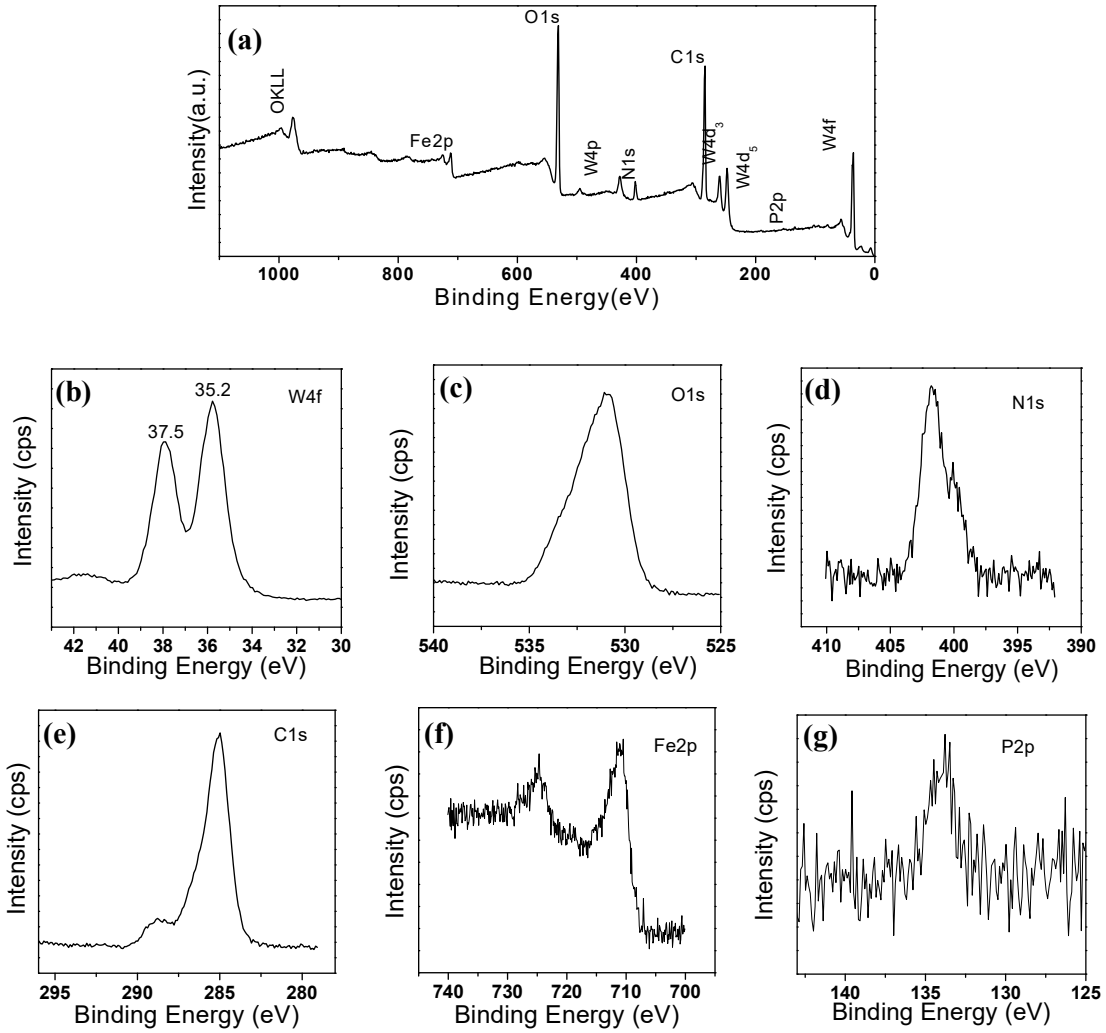

Figure S7. X-ray photoelectron spectra obtained for PTA@MMS: (a) Survey spectrum showing the characteristic peaks of C, N, Fe, W, P and O; Core level spectra for b) W4f, c) O1s, d) N1s, e) C1s, and f) P2p.

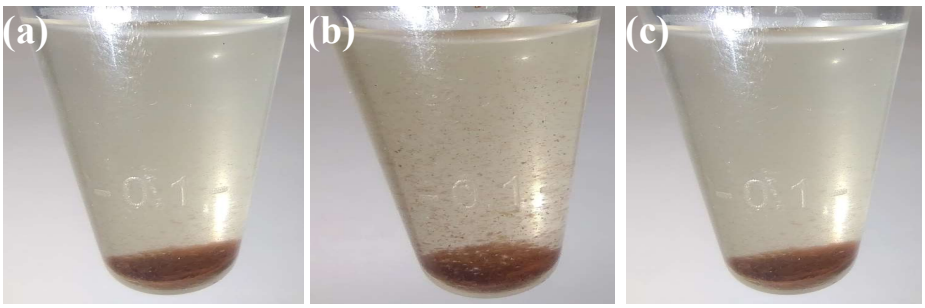

Figure S8. Photographic images of the reaction mixture used in benzyl alcohol oxidation in the presence of PTA@MMS as catalyst: a) Reaction mixture of CH_3CN, benzyl alcohol and PTA@MMS (settled at the bottom) before reaction; b) During the reaction; c) After the reaction (biphasic)

Figure S9. Photographic images of the reaction mixture used in benzyl alcohol oxidation in the presence of PTA@MMS as catalyst: a) Reaction mixture of water (bottom layer), benzyl alcohol (upper layer) and PTA@MMS (at the interface) before reaction; b) During the reaction; c) After the reaction (triphasic)

Table S4. Change in catalytic activity with variation in the amount of PTA@MMS catalyst in the oxidation of benzyl alcohol

Amount (mg)	Conversion (%)	Selectivity (%)
15	63.21	96
20	66.75	95.23
25	97.04	97.2
30	85.32	96.2

Conditions: BzOH- 1.0 mmol, H_2O_2 -1.5 mmol, 6 mL water, 90^{o}C, 15 h

Table S5. Change in catalytic activity with variation in the concentration of the substrate (benzyl alcohol) in its oxidation over PTA@MMS catalyst

Benzyl alcohol (mmol)	**Conversion (%)**	**Selectivity (%)**
0.2	51	99
1.0	97.04	97.2
5.0	69.45	88.4

Conditions: H_2O_2 -1.5 mmol, PTA ~5.0 μmol, 6 mL water, 90^{o}C, 15 h

Proposed Mechanism:

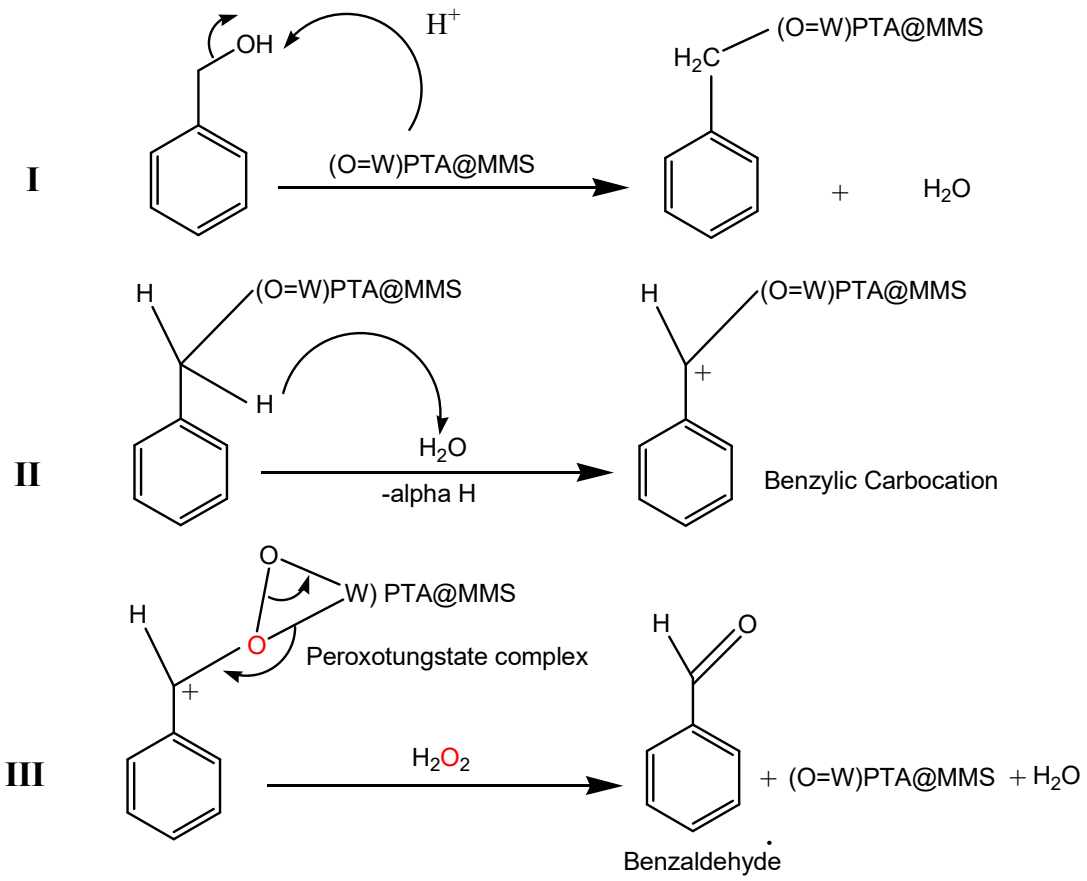

Figure S10. Schematic illustration of the plausible pathway for the oxidation of benzyl alcohol in the presence of PTA@MMS as catalyst.

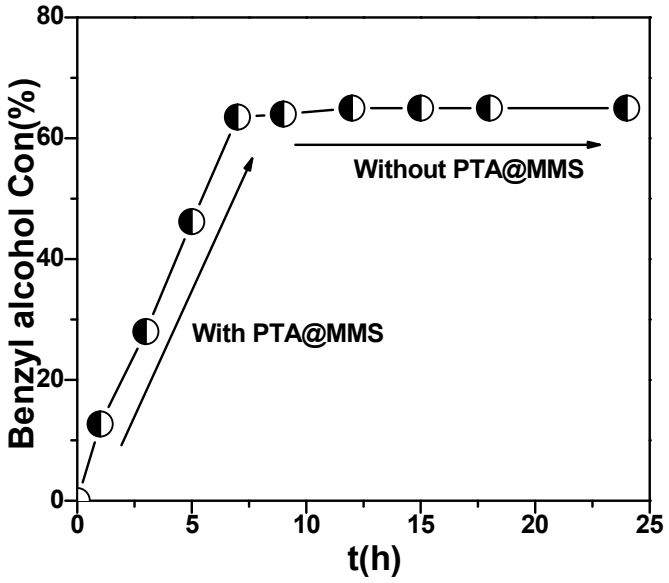

Figure S11. Plot of benzyl alcohol conversion with time in the presence of the PTA@MMS catalyst and after the catalyst is separated via hot-filtration from the reaction mixture during the catalytic reaction. (Reaction conditions: BzOH- 1.0 mmol, H_2O_2 -1.5 mmol, 6 mL water, 90^oC, 15 h).

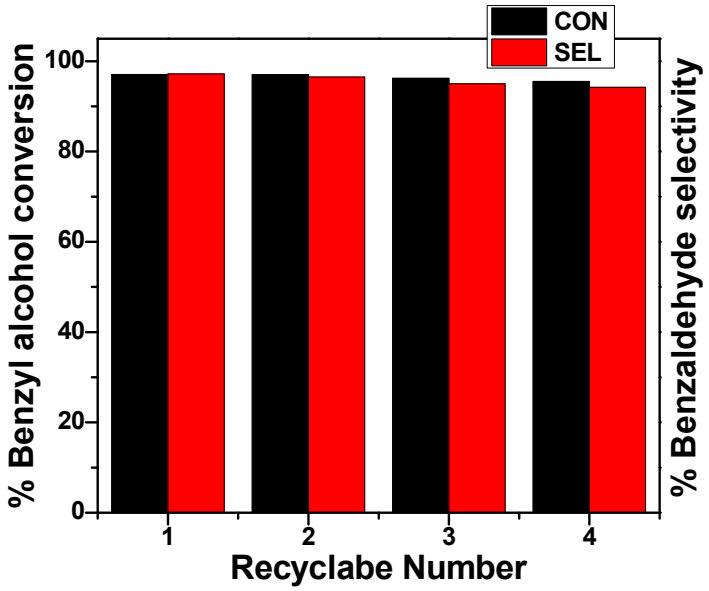

Figure S12. Catalytic activity and selectivity observed in the reusability test of PTA@MMS catalyst in the oxidation of benzyl alcohol reaction. (Reaction conditions: BzOH- 1.0 mmol, H_2O_2 -1.5 mmol, 6 mL water, 90^{o}C, 15 h)

Table S6: The amount of Tungsten (determined by ICP-OES of the solution diluted to 25 mL) present in the reaction mixture after the PTA@MMS catalyst is separated from the reactor via hot-filtration during different reaction cycles of benzyl alcohol oxidation. (Reaction conditions: 1.0 mmol BzOH, 1.5 mmol H_2O_2, 6 mL water, 90^oC, 15 h)

Catalyst	**Concentration of W present in the reaction mixture (ppm)**	**Loss in W amount (%)**
1st Cycle	2.3±0.1	0.130
2nd Cycle	1.93±0.1	0.110
3rd Cycle	0.61±0.1	0.034
4th Cycle	0.12±0.1	0.007

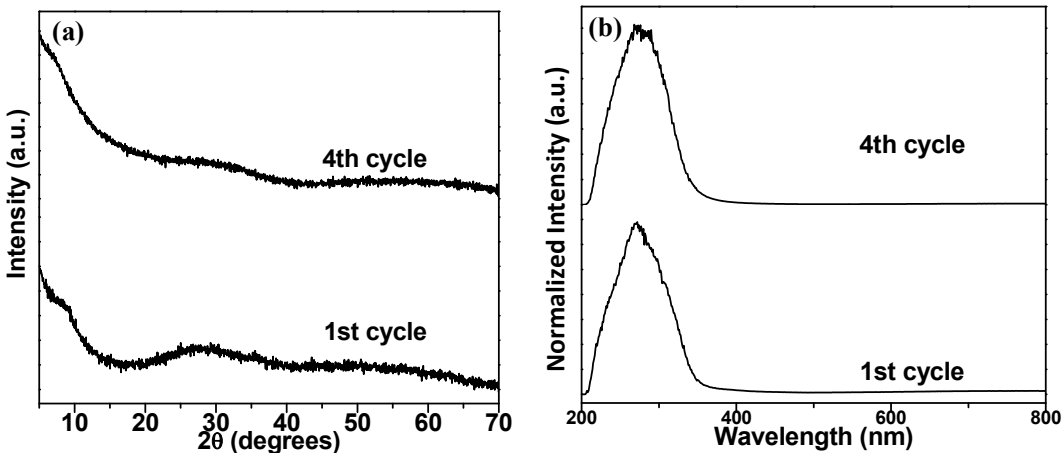

Figure S13. a) XRD pattern; b) UV-vis DRS spectra of the recycled PTA@MMS catalyst used at various reaction cycles for the oxidation of benzyl alcohol reaction.

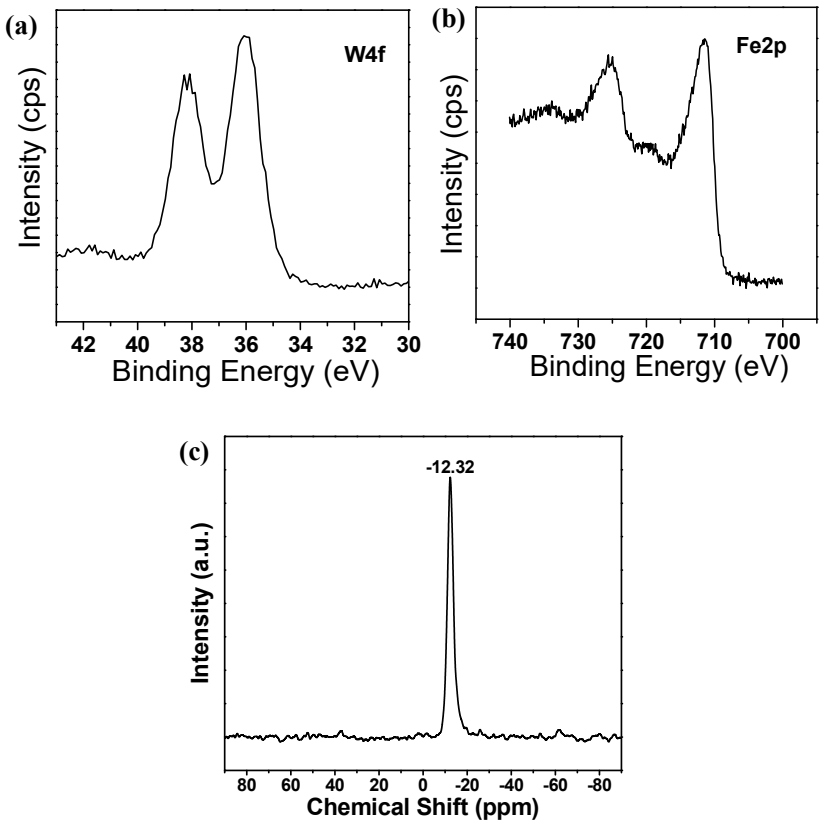

Figure S14. XPS core level spectra of (a) W4f, and (b) Fe 2p; c) ^{31}P NMR spectrum of the recycled PTA@MMS catalyst in the oxidation of benzyl alcohol reaction.

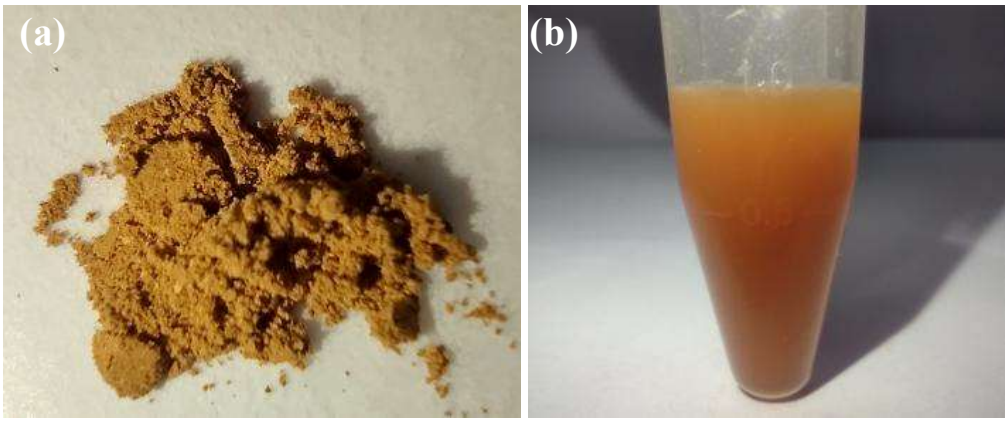

Figure S15. Photographic images of a) dried sample of PTA@MMS, and b) an aqueous suspension of PTA@MMS.

Table S7. Comparison of the catalytic activities of PTA@MMS with other reported phosphotungstate-based catalysts for benzyl alcohol (BzOH) oxidation with H_2O_2

S.N	Catalyst	Reaction conditions	BzOH Oxidation*		*TON	Ref.
			Con %	Sel %		
1	PIPA-n	Alcohol 10 mmol, 15 mmol (30%) H_2O_2, 1.3 mol% catalyst, 95 °C, water (1.5 mL)	96	86	73.84	S3
2	SiO_2-BisILs[$W_2O_3(O_2)_4$]	Alcohol (1 mmol), H_2O_2 (1.4mmol), catalyst (1 mol%), 90°C,18h, water (2mL)	98	96	98.0	S4
3	GO/Fe_3O_4/HPW	Alcohol (1 mmol), catalyst (20 mg), H_2O_2 (5 mmol), 70 °C.	99	100	142.6	S5
4	Fe_3O_4@SiO_2/NH-$PW_{10}V_2O_{40}$	Catalyst (20 mol%, 0.02 g), alcohol (1.0 mmol), H_2O_2 (2 ml), toluene (2 ml), 80 °C	98	99	141.2	S6
5	GO/Im-$PW_{12}O_{40}^{3-}$	Catalyst (0.6 g), alcohol (40 mmol), H_2O_2 (100 mmol), 90 °C	90	99	172.4	S7
6	PW11/MP	Alcohol 20mmol, H_2O_2 (20mmol) catalyst PW11/MP 10 wt% w.r.t alcohol, 90 °C, 18 h. 6 ml of CH_3CN	94.2	69.8	188.4	S8
7	$[TMGHA]_{2.4}H_{0.6}PW$	Alcohol (10 mmol), 30 wt % H_2O_2 (15 mmol), catalyst (0.03 mmol), 6 mL, water, 90 °C	97.9	93.5	323.3	S9
8	PTA- Jeffamine	Catalyst (0.5 g), alcohol (1.9M), H_2O_2 (3.9M), 90 °C	100	59	10.98	S10
9	PW4/DAIL/MIL-100(Fe)	Alcohol (1 mmol), oxidant (4.5 mmol), TBHP/$CHCl_3$, catalyst 6 µmol, 100 °C.	92	99	153.3	S11
10	$[DEDSA]_3PW_{12}O_{40}$	Alcohol (1 mmol), H_2O_2 (3 mmol), $[DEDSA]_3PW_{12}O_{40}$ (3.5 mol%), CH_3CN (2 mL), 65°C, 6h	97.5	88.5	27.85	S12
11	$[C4mim]_4PMo_{11}VO_{40}$	Alcohol (30 mmol), 30 wt% H_2O_2 (36 mmol), catalyst (100 mg), water (6 mL), 80°C	34	99	186.0	S13
12	PW@IL-GO (1.5)	Alcohol (10 mmol), catalyst (0.15 mol%, (15.0 wt% H_2O_2), water (5 mL), 100 ◦C	94	91	626.0	S14
13	Im- PW/GO	Substrate 40 mmol, molar ratio of alcohol with H_2O_2 = 1:2.5, catalyst 0.6 g, 90◦C	90.8	99.2	173.0	S15
14	**PTA@MMS**	BzOH- 1.0 mmol, H_2O_2 -1.5 mmol, catalyst 5µmol, 6 mL water, 90°C	**97.0**	**97.2**	**194.0**	**This work**

*** Sel (%) is with respect to Benzaldehyde, TON = moles of substrate conversion/moles of catalyst**

References:

S1. Murugappan, K.; Silvester, D.S.; Chaudhary, D.; Arrigan, D.W.M. Electrochemical Characterization of an Oleyl-coated Magnetite Nanoparticle-Modified Electrode *CHEMELECTROCHEM*, 2014, **1**, 1211-1218. doi.org/10.1002/celc.201402012

S2. Ayyappan, S.; Gnanaprakash, G.; Panneerselvam, G.; Antony, M.P.; Philip, J. Effect of Surfactant Monolayer on Reduction of Fe_3O_4 Nanoparticles under Vacuum. *J. Phys. Chem. C* 2008, **112**, 18376–18383. doi.org/10.1021/jp8052899

S3. Hao, P; Zhang, M; Zhang, W; Tang, Z; Luo, N; Tan, R; Yin. D. Polyoxometalate-based Gemini ionic catalysts for selective oxidation of benzyl alcohol with hydrogen peroxide in water. *Catal. Sci. Technol.*, 2018, **8**, 4463-4473. doi.org/10.1039/C8CY01191E

S4. Fan, J; Pu, F; Sun, M; Liu, Z. W; Han, Wei, J. F; Shi, X. Y. Immobilized bis-layered ionic liquids/peroxotungstates as an efficient catalyst for selective oxidation of alcohols in neat water. *New J. Chem.*, 2016, **40**, 10498-10503. doi.org/10.1039/C6NJ01476C

S5. Darvishi, K; Amani, K; Rezaei, M. Preparation, characterization and heterogeneous catalytic applications of GO/Fe_3O_4/HPW nanocomposite in chemoselective and green oxidation of alcohols with aqueous H_2O_2. *Appl Organometal Chem*. 2018, **32**, 1-14. doi.org/10.1002/aoc.4323

S6. Dong, X; Zhang, X.; Wu, P.; Zhang, Y.; Liu, B.; Hu, H.; Xue, G. Divanadium-Substituted Phosphotungstate Supported on Magnetic Mesoporous Silica Nanoparticles as Effective and Recyclable Catalysts for the Selective Oxidation of Alcohols. *ChemCatChem* 2016, ***8***, 3680-3687. doi.org/10.1002/cctc.201601077

S7. Leng, Y.; Liu, J.; Jiang, P.; Wang, J. Heteropolyanion-based polymeric hybrids: highly efficient and recyclable catalysts for oxidation of alcohols with H_2O_2. *RSC Adv.* 2012, ***2***, 11653-11656. doi.org/10.1039/C2RA22348A

S8. Churipard, S. R.; Kanakikodi, K. S.; Choudhuri J. R.; Maradur. S. P. Polyoxotungstate ($[PW_{11}O_{39}]^{7-}$) immobilized on mesoporous polymer for selective liquid-phase oxidation of alcohols using H_2O_2. *RSC Adv*., 2020, **10**, 35988-35997. doi.org/10.1039/D0RA07178A

S9. Chen, G.; Zhou, Y.; Long, Z.; Wang, X.; Li, J.; Wang, J. Mesoporous Polyoxometalate-Based Ionic Hybrid As a Triphasic Catalyst for Oxidation of Benzyl Alcohol with H_2O_2 on Water. *ACS Appl. Mater. Interfaces* 2014, **6**, 4438−4446. doi.org/10.1021/am5001757

S10. Bhattacharjee, R. R.; Thangamani, S.; Mal. S S. A Liquid Derivative of Phosphotungstic Acid as Catalyst for Benzyl Alcohol Oxidation in Water: Facile

Separation and Stability of Benzaldehyde at Room Temperature. *ChemistrySelect* 2017, **2**, 4368 – 4375. doi.org/10.1002/slct.201700443

S11. Abednatanzi, S.; Abbasi, A.; Farahani. M. M. Immobilization of catalytically active polyoxotungstate into ionic liquid-modified MIL-100(Fe): A recyclable catalyst for selective oxidation of benzyl alcohol. *Catal. Commun.* 2017, **96**, 6–10. doi.org/10.1016/j.catcom.2017.03.011

S12. Kashyap, N.; Das, S.; Borah. R. Solvent responsive self-separation behaviour of Brønsted acidic ionic liquid-polyoxometalate hybrid catalysts on H_2O_2 mediated oxidation of alcohols. *Polyhedron* 2021, **196**, 114993-1145006. doi.org/10.1016/j.poly.2020.114993

S13. Tong, J.; Su, L.; Li, W.; Wang, W.; Ma, H.; Wang, Q. Hybrids of $[C_4mim]_{3+x}PMo_{12-x}V_xO_{40}$: A new catalyst for oxidation of benzyl alcohol to benzaldehyde in water with greatly improved performances. *Polyhedron* 2016, **115**, 282–287. doi.org/10.1016/j.poly.2016.05.024

S14. Zheng, W.; Wu, M.; Yang, C.; Chen, Y.; Tan, R.; Yin. D. Alcohols selective oxidation with H_2O_2 catalyzed by robust heteropolyanions intercalated in ionic liquid-functionalized graphene oxide. *Mater. Chem. Phy.* 2020, **256**, 123681-124688. doi.org/10.1016/j.matchemphys.2020.123681

S15. Zhang, W. H.; Shen, J. J.; Wu, J.; Liang, X. Y.; Xu, J.; Liu, P.; Xue, B.; Li, Y. X. An amphiphilic graphene oxide-immobilized polyoxometalate-based ionic liquid: A highly efficient triphase transfer catalyst for the selective oxidation of alcohols with aqueous H_2O_2. *Mol. Catal.* 2017, ***443***, 262-269. doi.org/10.1016/j.mcat.2017.10.018